Mutlilayer Wedge Disks CROW for an Optical Delay Line

Marc-Antoine Bianki[1*], Cédric Lemieux-Leduc[1], Régis Guertin[1], and Yves-Alain Peter[1]

***Abstract*—Optical delay lines are vital for the development of all optical telecommunications, optical computers and for many nonlinear and quantum optics processes. Periodic structures such as coupled resonator optical waveguides (CROW) achieve high delays in a compact manner and with a large bandwidth. Wedge disk resonators have demonstrated high quality factors compared to rectangular disks and rings while remaining integrable on chip. Vertical coupling is needed since the optical mode is pushed toward the disk center by the wedge. We propose an optical delay line made of wedge disks arranged in two overlapping layers. Disks are made of silicon dioxide on silicon pillars. Numerical calculations of the device performance and an experimental proof of concept are presented. A maximum delay of $85\,\mathrm{ps}$ for eleven disks is achieved with a loss per cavity of $3.91\,\mathrm{dB}$. This is a first proof of concept of a CROW structure made of wedge disk coupled vertically.**

***Index Terms*—Coupled-resonator optical waveguide, Multilayer photonic, Optical Memory, Slow light, Vertical coupling, Wedge disk, Whispering Gallery Modes Resonator**

I. Introduction

Slow light has many applications from telecommunications to quantum optics. In an optical computer or router, information transmitted by light must be temporally stored in an optical memory [1]. Since light-matter interactions are weak, fields like quantum photonics and non-linear optics benefit from slow light [2]. Optical delay lines are also useful for phased array antennas [3]–[5] and gyroscopes [6].

There are different ways to generate an optical delay with passive structures such as long waveguides folded into a spiral to reduce the device footprint. Low loss per delay is achieved with a high bandwidth, but the footprint remains large [7]. A dispersion structure has a lower group velocity of light. It is smaller than the spiral and achieves similar optical delays. However, bandwidth is smaller. Bragg gratings can be used as dispersion engineered structures [8]. Resonant structures have also a low group velocity, but with a larger bandwidth than the dispersion structures. They are a good compromise between footprint and bandwidth and they usually take the form of coupled resonators optical waveguides (CROWs) or side-coupled integrated spaced sequences of optical resonators (SCISSORs). Light propagates in each resonator which can be Fabry-Perot, rings, photonic crystals or disks.

The proposed design aims to have a small footprint, a reasonable bandwidth, and a large delay with low losses. As the device is passive, there is no amplification and ways to change the delay. A CROW made of disk resonators is chosen for their high quality factor (Q) [9] and their integrability. Wedged disks are wet etched in order to lower losses. The optical resonant mode is pulled towards the disk center due to the wedge. Since the amplitude of the whispering gallery mode is smaller at the edge, the optical losses due to surface scattering decrease. The resonator quality factor is thus increased [10]. The wedge comes from the peel-off of the resist during wet etching [11]. The final angle between the linear profile and the disk base is called the Mach angle. It is controlled by the peel-off velocity, which depends on the resist adhesion to the substrate. With this design, horizontal coupling is not optimal. Therefore, we use a 3D photonics approach with multiple layers optical structures which can enable an efficient vertical coupling. This technique increases the component density [12], and waveguide crossing is also possible [13]. Vertical coupling has been achieved between a straight waveguide and a wedge disk resonator [14]–[16]. One of the advantages of vertical coupling compared to horizontal coupling are larger misalignment tolerances [17]. In addition, the wedge geometry limits the feasibility of lateral coupling. Figure 1 shows a typical configuration of our proposed approach. It is composed of silica wedge disks arranged in two layers and coupled vertically by overlapping the adjacent disk edges to form a CROW. Disks stand on silicon pillars and light is coupled in and out of the CROW using tapered optical fibers.

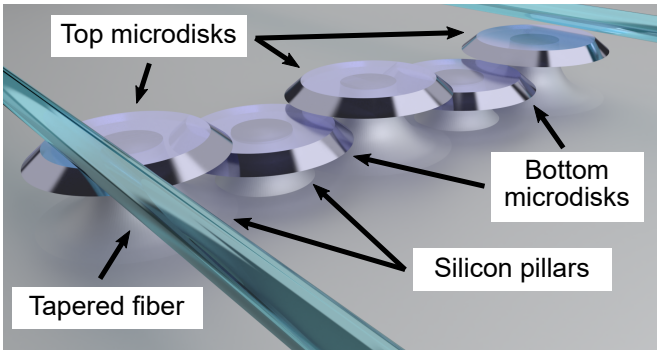

Fig. 1. Device schematic. It is composed of overlapping silica microdisks arranged in two layers (top and bottom) and supported with silicon pillars. Tapered optical fibers are used to inject and collect the transmitted light.

II. Theoretical Model

An optical microdisk resonator of radius R has resonant wavelengths λ_m, which are a multiple of the optical path

[1] Department of Engineering Physics, Polytechnique Montréal, Montréal, Québec, Canada
[*] Corresponding author : marc-antoine.bianki@polymtl.ca
This work was supported in part by the Fonds de recherche du Québec - Nature et technologies (FRQNT), (206058), and the Natural Sciences and Engineering Research Council of Canada (NSERC), [RGPIN-2020-06692].

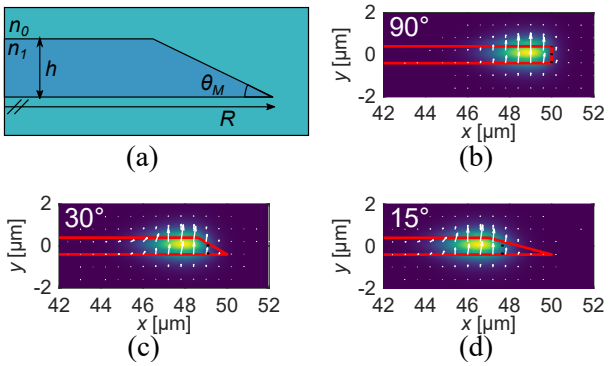

Fig. 2. Numerical mode calculation. (a) simulated geometry, (b), (c) and (d), transverse magnetic (TM) intensity fields calculated for Mach angles 90°, 30° and 15° respectively and a resonance frequency at 1.55 µm. White arrows are the electric field in the xy plane.

length $m\lambda_m = 2\pi R n_{\text{eff}}$ where n_{eff} is the resonance mode effective refractive index. The free spectral range separating each resonance peak is $\lambda_{\text{FSR}} = \lambda^2/2\pi R n_{\text{eff}}$. Its full width at half-maximum (FWHM) is $\delta\lambda = \lambda/Q$ where Q is the quality factor, which is inversely proportional to the losses. Wedge disk resonators cannot be resolved with the scalar approximation. Mode calculation with vectorial theory is required. Modes were calculated numerically with the weak form of the Maxwell equations considering the axial symmetry [18]. Therefore, only the cross-section (xy plane) is calculated. Examples of calculated modes are given in Fig. 2 for multiple Mach angles θ_M. The calculations provide the resonance wavelength with its mode field distribution. It is observed that optical modes are pushed towards the center as the angle decreases. An effective radius R_{eff} is defined as the radius of an equivalent rectangular disk resonator where the mode field maximum is at the same position as the wedge disk. Then, with the resonance condition, the effective refractive index is obtained.

The difference between horizontal and vertical coupling is shown in Fig. 3 (a). A top view and side view of the two configurations are represented. For horizontal coupling, disks are in the same plane and separated by Δx. For vertical coupling, disks are overlapped by Δx and vertically separated by s. The refractive index of both disks are n_1 and n_2 and the background refractive index is n_0. The distance d between the modes is not constant along the light pathway position inside a disk. It is minimum at the overlap, but modes go away from each other away from the overlap. For large disks compared to the minimum separation distance, the vertical coupling is similar to two straight waveguides of propagation constant β. Since the propagation direction is parallel (flat zone) over an effective coupling length L_{eff}, the coupled-mode theory is used. In the coupling region, the modes of each disk overlap with each other. In the side view, we can see the modes overlap at the coupling point (horizontal coupling) or region (vertical coupling). L_{eff} is calculated similarly for a disk and a straight waveguide [19]. d is calculated from the geometry and along the light pathway. As it is shown in the graphic of Fig. 3 (b), a quasi-constant separation is obtained for vertical coupling that is not obtained with horizontal coupling. Over this section, coupling coefficients C_{ij} are given with the field overlap integrals (Side view):

$$C_{ij} = \frac{k_0^2}{2\sqrt{|\beta_i \beta_j|}} \int_{A_\infty} \left(n^2 - \bar{n}^2\right) \hat{\Psi}_i^* \hat{\Psi}_j dA \qquad (1)$$

where k_0 is the wave number, n and $\bar{n}$ are the refractive indices with and without the other waveguide respectively, Ψ is the normalized field amplitude and A is the transversal plane.

From the weak coupling approximation, and over L_{eff} (Fig. 3), the coupling factor κ is given by:

$$\kappa = \frac{C_{21}}{i\gamma} \exp\left(i\frac{\Delta\beta L_{\text{eff}}}{2}\right) \sin(\gamma L_{\text{eff}}) \qquad (2)$$

where $\Delta\beta = \beta_2 - \beta_1$ and $\gamma^2 = \left(\frac{\Delta\beta}{2}\right)^2 + C_{12}C_{21}$.

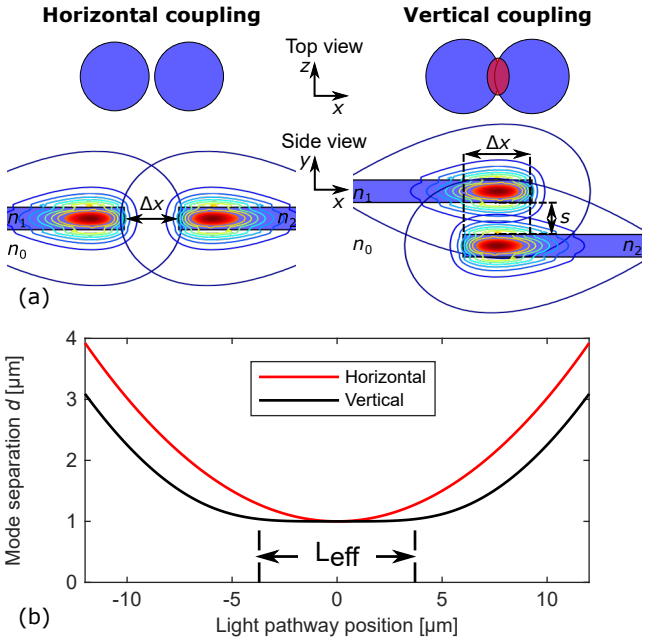

Fig. 3. (a) Schematics of side and top views of horizontal and vertical coupling (b) Mode separation d along the light pathway position for a horizontal (red) and a vertical (black) coupling. Disks have a radius of 50 µm and the minimum separation in both cases is 1 µm

The vertical coupling factor κ is computed versus the vertical s and horizontal Δx separations (Fig. 4 (a) and (b) respectively) for both transverse magnetic (TM) (dashed) and transverse electric (TE) modes (solid). For the horizontal alignment, maximal coupling is achieved when mode field maximums are aligned. For vertical separation, an oscillatory regime with small vertical separation s is explained by a smaller coupling length $L_C = 2\pi/C_{ij}$ than the effective coupling length L_{eff}. L_C is the length after which the total power transferred from one resonator to the other. When these two lengths are equal, marked by vertical lines in (b), the coupling factor decreases exponentially. Since the separation distance comes from layer thickness, there is no need for high-resolution lithography. TM polarization coupling factor is larger than TE polarization outside the oscillation regime. It is explained by the mode field distribution, which is more

vertically elongated for TM polarization since the electric field is continuous at interfaces.

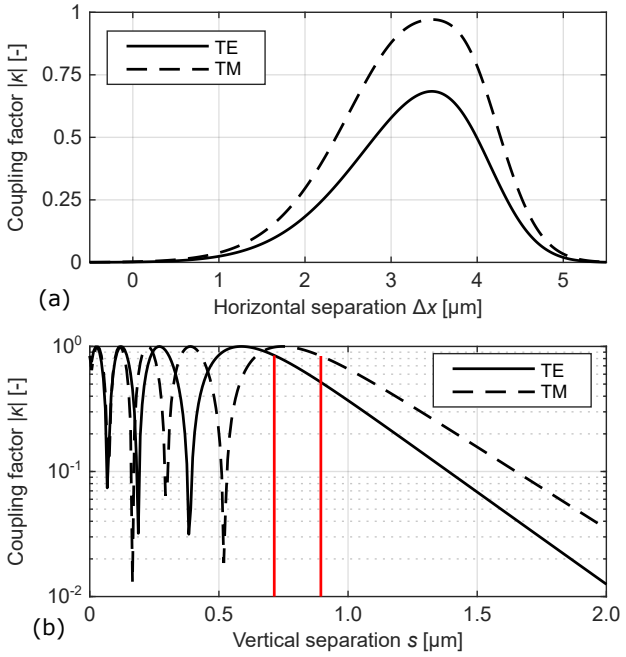

Fig. 4. Vertical coupling factor $|\kappa|$ versus (a) overlap Δx and (b) vertical separation s for both transverse magnetic (TM) (dashed) and transverse electric (TE) modes (solid). The vertical line in (b) are where the coupling length L_C is equal to the effective coupling length L_{eff}

The CROW transfer function is calculated with the matrix method [20]. The transfer matrix $\mathbf{P}$ depends on the coupling factor κ with $|t|^2 + |\kappa|^2 = 1$. The propagation matrix $\mathbf{Q}$ depends on the complex propagation constant β and disk radius R. Complex amplitudes a_i and b_i of the power of each disk ($i = 1, 2, .., N$) before and after the coupling are calculated as well as the waveguides ($i = 0, N+1$) as shown in Fig. 5 (a).

$$\begin{bmatrix} a_{i+1} \\ b_{i+1} \end{bmatrix} = \mathbf{PQ} \begin{bmatrix} a_i \\ b_i \end{bmatrix} \tag{3}$$

$$\mathbf{P} = \frac{1}{\kappa} \begin{bmatrix} -t & 1 \\ -1 & t* \end{bmatrix} \tag{4}$$

$$\mathbf{Q} = \begin{bmatrix} 0 & e^{-i\beta R\pi} \\ e^{i\beta R\pi} & 0 \end{bmatrix} \tag{5}$$

The total transmission $T = |t|^2 = |b_{N+1}/a_0|^2$ is given by

$$\begin{bmatrix} a_{N+1} \\ 0 \end{bmatrix} = (\mathbf{PQ})^N \mathbf{P} \begin{bmatrix} a_0 \\ b_0 \end{bmatrix} \tag{6}$$

Figure 5 (b) presents the delay per cavity and loss per cavity versus the coupling factor κ for different quality factors Q. There is a compromise between delay and loss. A plateau of the delay per cavity is observed for small coupling factor and its amplitude depends on the quality factor. For the loss per cavity, a turning point is located around the critical coupling, shown in green, for each quality factor. It is a good trade-off for design purposes. In summary, the quality factor has to be increased first. Then, the optimal coupling factor is the critical parameter to maximize the delay.

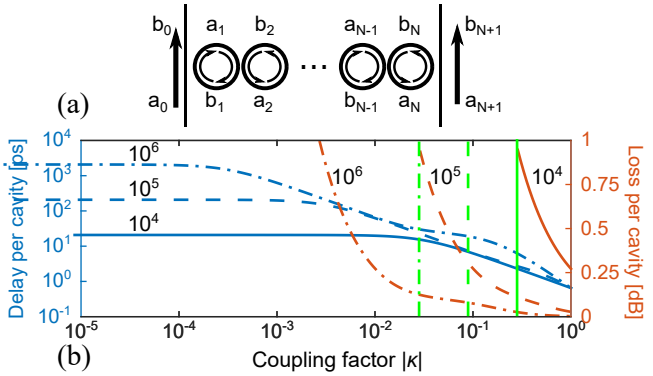

Fig. 5. (a) CROW illustration for matrix analysis (b) Delay and loss per cavity as function of coupling factor. Green lines show critical coupling

III. Microfabrication

The fabrication process is shown in Fig. 6 (a). It starts with the growth of 800 nm silicon dioxide (SiO_2) by wet thermal oxidation of a silicon wafer (Si) (step 1). A photolithography defines the bottom layer of disk resonators with a 50-μm radius. For subsequent steps, adhesion must be well controlled as it defines the wedge angle. A wet etch with hydrofluoric acid (7:1) of the resonators is performed until the silicon interface appears (step 2). The resist peel-off forms a disk Mach angle [11] which depends on the resist adhesion with the disk. More than 2 μm of amorphous silicon (a-Si) is deposited by sputtering (step 3) and a chemical mechanical planarization is used to remove any remaining structure and roughness (step 4). A 1.3-μm layer of amorphous silicon is left for the separation layer and the next step of oxidation of 800 nm of silicon oxide (step 5). A second lithography is used to define the top layer of disk resonators aligned with the previous lithography. An alignment tolerance of 1 μm is needed according to calculations shown in Fig. 4 (a). A wet etch is realized on the top layer (step 6). The disks are under etched and pillars are formed by a reactive ion etching with a sulfur hexafluoride (SF_6) plasma (step 7). An undercut of 15 μm is obtained.

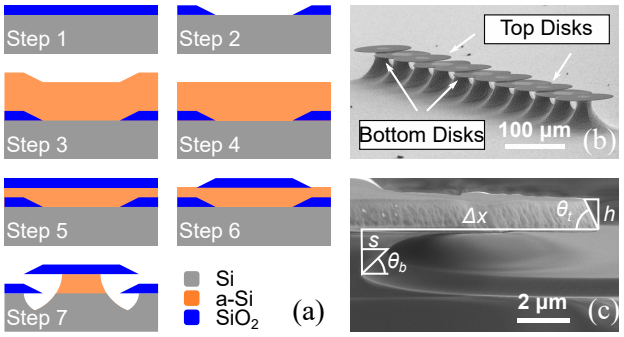

Fig. 6. Microfabrication (a) process flow, (b) overall scanning electron micrograph, (c) close-up view of disks overlap.

A scanning electron micrograph overview of the fabricated delay line is shown in Fig. 6 (b). Two disk layers are shown

with overlaps of each adjacent disk. The eleven silicon dioxide disks have a radius R of $50\,\mu\mathrm{m}$ and lay on a silicon pillar. A second micrograph (Fig. 6 (c)) shows a close-up view of two adjacent disks overlap. The thickness h and Mach angle, θ_t and θ_b, of each disk, the overlap distance Δx and the separation thickness s are measured (Tab. I). Asymmetry between the two disk layers is explained by micromachining parameters deviations of amorphous silicon and thermal silicon oxide deposition, photolithography and wet etching steps. It has an impact on the optical response of the device, since the periodic unit extends from one to two cavities.

TABLE I
SCANNING ELECTRON MICROSCOPY MEASURED GEOMETRICAL PARAMETERS

Parameters		Values	Parameters		Values
R_t	[µm]	49.7	R_b	[µm]	48.8
h_t	[µm]	1.10	h_b	[µm]	0.8
θ_t	[°]	65	θ_b	[°]	40
Δx	[µm]	9	s	[µm]	0.7

IV. Optical Performance Characterization

Device characterization is performed with a Mach-Zehnder interferometer (Fig. 7 (a)). A tunable laser source (TLS) (AGILENT 81600B, AGILENT 8164B) is used with an optical isolator (I). A polarization controller (PC) is used to maximize the output power. Light is divided in the two arms of the interferometer with an optical coupler (C1). In the first arm, tapered optical fibers of $5\,\mathrm{cm}$ in length and $1\,\mu\mathrm{m}$ in diameter are used to inject and extract light at each end of the device (CROW). 5-axis micrometer stages are used to align and optimize the coupling between the tapered optical fibers and the structure. In the second arm, a mechanical delay line (MDL) is placed and is composed of two facing collimators with a variable separation δL achieved by two linear motorized stages. The length and the optical power are balanced between the two arms by varying the reference arm length and losses. A second coupler (C2) combines light from the two arms and a photodetector (D) (AGILENT 81634B) is synchronized with the tunable laser to record the spectrum.

The power spectrum of a device made of nine 50-$\mu\mathrm{m}$ radius cavities is shown in Fig. 7 (b) exhibiting no interference since the reference arm light is intentionally blocked. A periodic pattern of peaks with a period of $5.38\,\mathrm{nm}$ is observed. The $-3\,\mathrm{dB}$ bandwidth of the pattern is $3.2\,\mathrm{nm}$. Asymmetry of the two disk layers impacts the spectrum by dividing the pattern into two set of peaks with different powers. Since the top and bottom disks have different geometries, the resonant wavelengths are different, which has the effect of decreasing the bandwidth.

Losses are evaluated by placing the second tapered optical fiber to couple light out of the 3rd, 5th, 7th, 9th and 11th cavity with no interference. A single peak is evaluated around $1548.5\,\mathrm{nm}$ (Fig. 8 (a)). Losses versus the number of cavities of the CROW are reported in Fig. 8 (c). Losses of $-3.91\,\mathrm{dB}$ per cavity is computed using a linear regression.

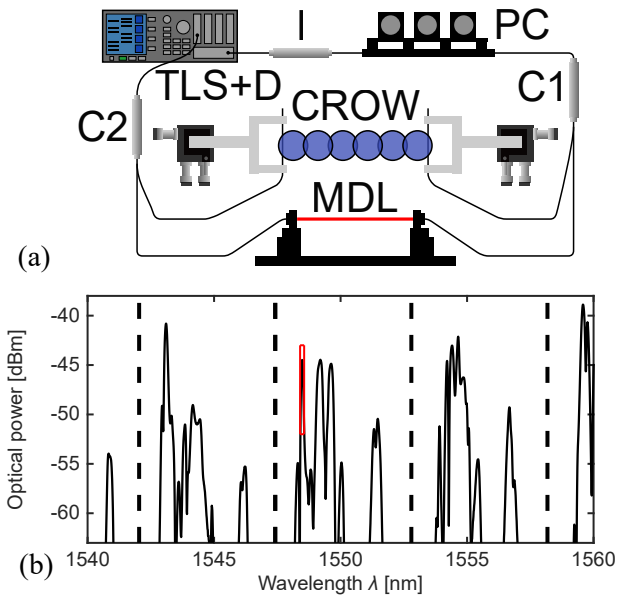

Fig. 7. Optical characterizations. (a) experimental setup, (b) experimental power spectrum with the chosen peak for loss and delay measurements in red

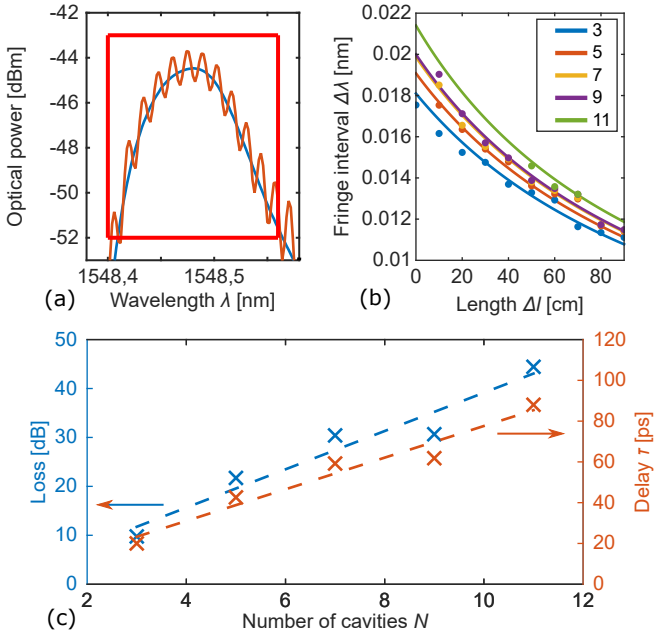

Fig. 8. Optical characterization. (a) close-up of the chosen peak with (orange) and without (blue) interference, (b) fringe interval $\Delta\lambda$ while varying length Δl for different CROW lengths, (c) delay and losses as function of number of cavities N

This procedure is repeated with interference. For each CROW length, a spectrum is taken, from which, wavelength fringes are measured as it is shown in Fig. 8 (a). They are due to the phase difference between the two signals. The fringe intervals $\Delta\lambda$ depend on the wavelength λ_0 and the optical path length difference ΔL:

$$\Delta\lambda = \frac{\lambda_0^2}{\Delta L} \tag{7}$$

By adding a varying length Δl to the mechanical delay line, we can fit the equation to obtain the relative optical path length difference.

$$\Delta\lambda = \frac{\lambda_0^2}{\Delta L + \Delta l} \tag{8}$$

The procedure is shown with Fig. 8 (b). Multiple measurements of fringe intervals are taken for different lengths and a regression is applied.

This procedure is reproduced for different numbers of resonators. The associated delay τ is taken with the refractive index of air ($n = 1$) as:

$$\Delta\tau = \frac{c}{n\Delta L} \tag{9}$$

From the linear regression, a delay per cavity of $7.76\,\mathrm{ps}$ in vacuum is obtained which is related to a slowdown factor of 5.8. From Fig. 5 (b), the corresponding coupling factor is around 0.17 which is lower than expected for a $0.7\,\mu\mathrm{m}$ separation. From Fig. 4 (b), the coupling factor should be around 0.88 for TE modes and 0.97 for TM modes. For 11 cavities, a maximal delay of $85.36\,\mathrm{ps}$ is achieved with losses of $43\,\mathrm{dB}$.

Based on the calculations from Fig. 5 (b), the quality factor is in the order of 1×10^4. To maximize the slowdown factor, a lower coupling coefficient is required. The main limitation remains losses, which come from fabrication deviations and material quality.

V. Discussion and Conclusion

The device performance is compared to the literature with a horizontal coupled disk CROW (Bergeron [21]) and a horizontally coupled ring CROW (Melloni [22]) (table II). Both are passive CROW structures. The first device is made of seven disks coupled horizontally. Disks are in silica on silicon pillars with the same thickness but with smaller radius ($35\,\mu\mathrm{m}$). Disks have a rectangular profile. The second device is made of eight ring resonators coupled horizontally. It has the particularity to be tunable with microheaters. It is also used in reflection. Resonator number is in the same order of magnitude for the three devices. Losses are smaller for the ring resonators, although disk resonators have potentially lower losses than ring resonators. The largest slowdown factor is obtained by rectangular disks. The coupling coefficient is likely to be lower than this work. An important figure of merit for an optical delay line is the delay per loss. It is higher for the ring resonator structure, but with a larger footprint. Rectangular disks are still better than this work, but the two disk-based designs have the advantage of a more compact optical delay line.

TABLE II
Comparison of device performances

	Microdisks Bergeron [21]	Rings Melloni [22]	Microdisks This work
Coupling	Horizontal	Horizontal	Vertical
Maximal delay [ps]	200.9	800	85.4
Loss per cavity [dB]	6.13	1.00	3.91
Slowdown factor S [-]	59.3	10.0	5.8
Number of cavities [-]	7	8	11
Delay per loss [ps/dB]	4.76	100	2
Area [mm^2]	0.035	7	0.101

The limiting factor with passive CROW structure for delay line applications is losses. This design has the advantage to integrate a high quality factor cavity within a CROW structure. Wedge disks alone have reached a high quality factor of 9×10^8 [10]. However, the repeatability of the wedge structure remains a fabrication challenge. The angle depends on the resist adhesion which depends on the etched material, the etching solution, the resist and its application. Other fabrication steps must be taken care of to obtain identical disks on both layers. The thickness and radius also have to be the same. If not, the resonance condition will be different and the bandwidth will decrease.

While this is a proof-of concept, this work opens the path to many improvements. For now, the coupling in and out of the structure is done with tapered optical fibers of a few microns thick. Using a silicon nitride on silicon dioxide platform [23], additional layers of photonic structure could be added while maintaining low propagation losses. Waveguides on a third layer could couple light underneath the first and last resonators. The same wedge angle could be obtained with this platform [14]–[16]. By using a passive design, we have shown the feasibility of this structure. To improve it, we could add microheaters and use the CROW in reflection. By detuning the last resonators, we can achieve a discrete variable delay as with ring resonators [22]. With a bulk nitride platform, heaters can be patterned on top microdisks. A solution to compensate losses could be to use an active material. By pumping the gain medium, a higher delay can be obtained for the same amount of losses [24]–[26].

In conclusion, the proof of concept of a novel optical delay line is presented. Design, simulation, fabrication, and characterization of the prototype of a delay line based on vertically coupled wedge disk resonators were achieved. With this work, we explored a novel structure using the high quality factor and integrability of wedge disks in a coupled-resonator optical waveguide. To overcome the coupling challenge, we have proposed and shown that vertical coupling can be achieved between these resonators. Calculations showed that the cavity losses are the main limiting factor for a passive CROW delay line. When it is optimized, the coupling factor must be tuned to be critical in order to achieve the largest delay per loss. To our knowledge, it is the first CROW made of wedge disks arranged between two layers and coupled vertically. Transmission through an 11-resonators device was realized with losses of $43.01\,\mathrm{dB}$ and an optical delay of $85.36\,\mathrm{ps}$.

REFERENCES

[1] A. Alduino and M. Paniccia, "Interconnects: Wiring electronics with light," *Nature Photonics*, vol. 1, no. 3, p. 153, 2007.
[2] T. F. Krauss, "Why do we need slow light?" vol. 2, pp. 448–450, 2008.
[3] G. Grosskopf, "Silica based optical beam former for 60 GHz array antennas," *Fiber and Integrated Optics*, vol. 22, no. 1, pp. 35–46, Jan. 2003.
[4] I. Frigyes and A. Seeds, "Optically generated true-time delay in phased-array antennas," *IEEE Transactions on Microwave Theory and Techniques*, vol. 43, no. 9, pp. 2378–2386, 1995.
[5] Y. Liu, A. R. Wichman, B. Isaac, J. Kalkavage, E. J. Adles, T. R. Clark, and J. Klamkin, "Ultra-Low-Loss Silicon Nitride Optical Beamforming Network for Wideband Wireless Applications," *IEEE Journal of Selected Topics in Quantum Electronics*, vol. 24, no. 4, pp. 1–10, Jul. 2018.
[6] S. Srinivasan, R. Moreira, D. Blumenthal, and J. E. Bowers, "Design of integrated hybrid silicon waveguide optical gyroscope," *Optics Express*, vol. 22, no. 21, p. 24988, Oct. 2014.
[7] H. Lee, T. Chen, J. Li, O. Painter, and K. J. Vahala, "Ultra-low-loss optical delay line on a silicon chip," *Nature Communications*, vol. 3, no. 1, Jan. 2012.
[8] W. Shi, V. Veerasubramanian, D. Patel, and D. V. Plant, "Tunable nanophotonic delay lines using linearly chirped contradirectional couplers with uniform bragg gratings," *Optics Letters*, vol. 39, no. 3, p. 701, Jan. 2014.
[9] D. Rafizadeh, J. P. Zhang, S. C. Hagness, A. Taflove, K. A. Stair, S. T. Ho, and R. C. Tiberio, "Waveguide-coupled AlGaAs/GaAs microcavity ring and disk resonators with high finesse and 216-nm free spectral range," *Optics Letters*, vol. 22, no. 16, p. 1244, Aug. 1997.
[10] H. Lee, T. Chen, J. Li, K. Y. Yang, S. Jeon, O. Painter, and K. J. Vahala, "Chemically etched ultrahigh-Q wedge-resonator on a silicon chip," *Nature Photonics*, vol. 6, no. 6, pp. 369–373, May 2012.
[11] M. Ghulinyan, M. Bernard, R. Bartali, and G. Pucker, "Formation of mach angle profiles during wet etching of silica and silicon nitride materials," *Applied Surface Science*, vol. 359, pp. 679–686, 2015.
[12] M. Hochberg and T. Baehr-Jones, "Towards fabless silicon photonics," *Nature Photonics*, vol. 4, no. 8, pp. 492–494, Aug. 2010.
[13] K. Shang, S. Pathak, B. Guan, G. Liu, and S. J. B. Yoo, "Low-loss compact multilayer silicon nitride platform for 3d photonic integrated circuits," *Optics Express*, vol. 23, no. 16, p. 21334, Aug. 2015.
[14] M. Ghulinyan, R. Guider, G. Pucker, and L. Pavesi, "Monolithic whispering-gallery mode resonators with vertically coupled integrated bus waveguides," *IEEE Photonics Technology Letters*, vol. 23, no. 16, pp. 1166–1168, Aug. 2011.
[15] F. Ramiro-Manzano, N. Prtljaga, L. Pavesi, G. Pucker, and M. Ghulinyan, "A fully integrated high-Q whispering-gallery wedge resonator," *Optics express*, vol. 20, no. 20, pp. 22 934–22 942, Oct. 2012.
[16] D. Gandolfi, F. Ramiro-Manzano, F. A. Rebollo, M. Ghulinyan, G. Pucker, and L. Pavesi, "Role of edge inclination in an optical microdisk resonator for label-free sensing," *Sensors*, vol. 15, no. 3, pp. 4796–4809, Feb. 2015.
[17] D. D. John, M. J. R. Heck, J. F. Bauters, R. Moreira, J. S. Barton, J. E. Bowers, and D. J. Blumenthal, "Multilayer platform for ultra-low-loss waveguide applications," *IEEE Photonics Technology Letters*, vol. 24, no. 11, pp. 876–878, Jun. 2012.
[18] M. Oxborrow, "Traceable 2-D finite-element simulation of the whispering-gallery modes of axisymmetric electromagnetic resonators," *IEEE Transactions on Microwave Theory and Techniques*, vol. 55, no. 6, pp. 1209–1218, 2007.
[19] M. Ghulinyan, F. Ramiro-Manzano, N. Prtljaga, R. Guider, I. Carusotto, A. Pitanti, G. Pucker, and L. Pavesi, "Oscillatory vertical coupling between a whispering-gallery resonator and a bus waveguide," *Physical review letters*, vol. 110, no. 16, p. 163901, 2013.
[20] J. Poon, J. Scheuer, S. Mookherjea, G. T. Paloczi, Y. Huang, and A. Yariv, "Matrix analysis of microring coupled-resonator optical waveguides," *Optics Express*, vol. 12, no. 1, p. 90, 2004.
[21] S. Bergeron, F. Vanier, and Y. A. Peter, "Silica microdisk coupled resonator optical waveguide," in *Proc. IEEE/LEOS Int. Conf. Optical MEMS and Nanophotonics*, Aug. 2009, pp. 73–74.
[22] A. Melloni, F. Morichetti, C. Ferrari, and M. Martinelli, "Continuously tunable 1 byte delay in coupled-resonator optical waveguides," *Optics letters*, vol. 33, no. 20, pp. 2389–2391, 2008.
[23] P. Muñoz, G. Micó, L. Bru, D. Pastor, D. Pérez, J. Doménech, J. Fernández, R. Baños, B. Gargallo, R. Alemany, A. Sánchez, J. Cirera, R. Mas, and C. Domínguez, "Silicon nitride photonic integration platforms for visible, near-infrared and mid-infrared applications," *Sensors*, vol. 17, no. 9, p. 2088, Sep. 2017.
[24] M. Moralis-Pegios, G. Mourgias-Alexandris, N. Terzenidis, M. Cherchi, M. Harjanne, T. Aalto, A. Miliou, N. Pleros, and K. Vyrsokinos, "On-chip SOI delay line bank for optical buffers and time slot interchangers," *IEEE Photonics Technology Letters*, vol. 30, no. 1, pp. 31–34, Jan. 2018.
[25] Y. Xie, L. Zhuang, K.-J. Boller, and A. J. Lowery, "Lossless microwave photonic delay line using a ring resonator with an integrated semiconductor optical amplifier," *Journal of Optics*, vol. 19, no. 6, p. 065802, May 2017.
[26] P. Neveu, M.-A. Maynard, R. Bouchez, J. Lugani, R. Ghosh, F. Bretenaker, F. Goldfarb, and E. Brion, "Coherent population oscillation-based light storage," *Physical Review Letters*, vol. 118, no. 7, Feb. 2017.

Marc-Antoine Bianki received his B.Eng. degree and his M.A.Sc. degree in Engineering Physics from Polytechnique Montréal, in 2018 and 2019, respectively. His research interests include optical whispering gallery mode resonators and inkjet printing with polymers. He is currently pursuing his Ph.D. degree in Engineering Physics at Polytechnique Montréal under the direction of Pr. Yves-Alain Peter. Mr. Bianki was a recipient of the NSERC Postgraduate Scholarship – Doctoral in 2019.

Cédric Lemieux-Leduc received his B.Eng. degree and his M.A.Sc. degree in Engineering Physics from Polytechnique Montréal, in 2017 and 2019, respectively. He is currently pursuing his Ph.D. degree in Engineering Physics at Polytechnique Montréal. His research interests include applications based on optical microresonators and integrated photonics. Mr. Lemieux-Leduc was a recipient of the NSERC Postgraduate Scholarship – Doctoral in 2019.

Régis Guertin is currently pursuing his Ph.D. degree in Engineering Physics in the Microphotonics Laboratory at Polytechnique Montréal. He received his B.Eng. degree and his M.A.Sc. degree in Engineering Physics from Polytechnique Montréal, in 2017 and 2019, respectively. In 2016, he joined Pr. Yves-Alain Peter's laboratory where he has been working on microfabricated optical gas sensors. His research interests include optical resonators, gas detection, and microfabrication of optical components.

Yves-Alain Peter received his M.Sc. degree in physics and his Dr.Sc. degree from the University of Neuchâtel, Switzerland, in 1994 and 2001, respectively. In 1995, he joined the Department of Medical Radiobiology as a Research Associate at the Paul Scherrer Institute, Switzerland. From 1995 to 2001, he was a Graduate Research Assistant with the Applied Optics Group, Institute of Microtechnology, University of Neuchâtel. From 2001 to 2003, he was a Post-Doctoral Researcher with the Microphotonics Group, Stanford University. From 2003 to 2004, he was a Research and Development Engineer and a Project Leader with the Swiss Center for Electronics and Microtechnology, Switzerland. In 2004, he joined Polytechnique Montréal, Canada, where he is now Professor of Engineering Physics. His current research interests include microphotonics and micro-opto-electro-mechanical systems.